frontiers | Frontiers in Earth Science

ORIGINAL RESEARCH
published: 25 May 2022
doi: 10.3389/feart.2022.909107

Origin of Dolomite in Lacustrine Organic-Rich Shale: A Case Study in the Shahejie Formation of the Dongying Sag, Bohai Bay Basin

Ziru Zhao[1,2,3], Chunmei Dong[1,2,3], Pengjie Ma[1,2,3]*, Chengyan Lin[1,2,3], Guiang Li[1,2,3], Xinyu Du[1,2,3], Guoqiang Luan[1,2,3], Yinjun He[4] and Weibin Liu[5]*

[1]Department of Earth Sciences, China University of Petroleum (East China), Qingdao, China, [2]Key Laboratory of Reservoir Geology in Shandong Province, Qingdao, China, [3]Key Laboratory of Deep Oil and Gas, China University of Petroleum (East China), Qingdao, China, [4]CNOOC Research Center, CNOOC Tianjin Company, Tianjin, China, [5]Oil and Gas Survey, China Geological Survey, Beijing, China

OPEN ACCESS

Edited by:
Dongdong Liu,
China University of Petroleum, Beijing, China

Reviewed by:
Yixin Dong,
Chengdu University of Technology, China
Zhu Zhao Qun,
Hebei University of Engineering, China

***Correspondence:**
Chunmei Dong
lcydcm@upc.edu.cn
Pengjie Ma
mapengjie1989@gmail.com

Specialty section:
This article was submitted to Economic Geology, a section of the journal Frontiers in Earth Science

Received: 31 March 2022
Accepted: 02 May 2022
Published: 25 May 2022

Citation:
Zhao Z, Dong C, Ma P, Lin C, Li G, Du X, Luan G, He Y and Liu W (2022) Origin of Dolomite in Lacustrine Organic-Rich Shale: A Case Study in the Shahejie Formation of the Dongying Sag, Bohai Bay Basin. Front. Earth Sci. 10:909107. doi: 10.3389/feart.2022.909107

In most organic-rich shale reservoirs, dolomite is widely distributed and has different types and crystal sizes. However, the characteristics and formation mechanism of the dolomites in organic-rich shale are still poorly understood. Petrographic and geochemical analyses were performed to interpret the formation of dolomite in the lacustrine organic-rich shale of the Shahejie Formation, Dongying Sag, Bohai Bay Basin. Four types of dolomites, which represent episodic recrystallization, were classified based on crystal size and shape: 1) micritic dolomite (Dol-1), 2) sub-to euhedral (cloudy cores with clear rims) dolomite (planar-e) (Dol-2), 3) anhedral dolomite (coarse planar-s to nonplanar crystals) in phosphatic particles (Dol-3), and 4) fracture-filling anhedral dolomite (Dol-4). Dol-1 has nonplanar mosaic micritic crystals with irregular intercrystalline boundaries and dull cathodoluminescence (CL), suggesting dolomitization during the early burial stage. Dol-1 tends to occur under high paleosalinity and warm conditions. Furthermore, the syngenetic relationship, with abundant framboidal pyrite and gypsum, suggests that bacterial sulfate reduction (BSR) may influence the formation of Dol-1. The high content of Sr and low content of Mn/Sr also indicate less influence on burial. The Dol-2 crystals show cloudy cores with clear rims attributed to progressive dolomitization during burial. Dol-2 is always associated with the organic matter within the organic matter-rich lamina. The anhedral crystals and undulate (sweeping) extinction of Dol-3, which is usually encased by phosphatic particles in the organic-rich lamina, reflect the recrystallization affected by bacteria and the subsequent thermal evolution of organic matter. Dol-4 fulfills the abnormal pressure fractures crosscutting the earlier phases (Dol-1 and Dol-2) with undulate (sweeping) extinction and different rare earth element (REE) patterns. Dol-4 may be affected by hydrothermal fluids, which are influenced by the thermal evolution of organic matter. The $^{87}Sr/^{86}Sr$ values of the four types of dolomites similarly demonstrate the same dolomitizing fluids. Dol-1 to Dol-3 have similar REE patterns but are different from Dol-4, suggesting that Dol-4 likely resulted from circulation through basinal sediments instead of different fluids. Focusing on the origin of dolomite has been instrumental in understanding

the diagenetic evolution, fluid flow, and organic-inorganic interactions in organic-rich shale and, hence, the reservoir formation of shale oil.

Keywords: dolomite, organic-rich shale, lacustrine, formation, dongying sag

INTRODUCTION

Shale oil and gas resources are becoming the major sources of energy in transition to low carbon energy resources (Vengosh et al., 2014; Liu et al., 2019; Wu et al., 2019; Wu et al., 2020; Tian et al., 2021; Zeng et al., 2021a; Li et al., 2022). And dolomitic rocks are the major hosts for sedimentary ore deposits and conventional hydrocarbon reservoirs (Hsu, 1966; Davies, 1979; Braithwaite et al., 2004; Wu et al., 2020; Ma et al., 2021; Zeng et al., 2021b). However, the "dolomite problem" in the sedimentary realm is still a subject of long-standing interest and study (Shukla and Baker, 1988; Land, 1992; Braithwaite et al., 2004; Burns et al., 2010). Dolomite is an important component of most of the lacustrine shale oil reservoirs in China, with various types, abundant occurrences, and wide distributions, including the second member of the Kongdian Formation of the Cangdong sag (Pu et al., 2016), the upper part of the fourth member and the lower part of the third member of the Shahejie Formation of the Dongying sag (Ma et al., 2020), and the Fengcheng member of the Mahu sag (Tang et al., 2021). Although a series of dolomitization models (e.g., evaporative, seepage-reflux, hydrothermal dolomitization) have been established to demonstrate the formation of massive marine dolomites (Morrow, 1982; Warren, 2000; Machel, 2004), there are fewer studies on the formation of dolomite in organic-rich shales. Recently, researchers have found that various microbes have essential implications during dolomitization in natural sedimentary environments (Wright, 1999; Bontognali et al., 2014; Petrash et al., 2017), which are related to the formation of dolomite in organic-rich shales.

Organic material of microbial origin has been proven to catalyze dolomite precipitation in sedimentary systems, especially in shales (Vasconcelos et al., 2006; Bontognali et al., 2008; Bontognali et al., 2010; Diloreto et al., 2020). Organic matter degradation plays a vital role in dolomite dissolution and precipitation in shales (Irwin et al., 1977; Seewald, 2003). Organic matter degradation can be driven by various biotic and abiotic reactions, which significantly influence dolomitization fluids (Irwin et al., 1977; Mazzullo, 2000; Petrash et al., 2017). Previous studies have shown a close relationship between dolomite formation in shales and depositional environments, microbial activities, and progressive burial diagenesis (Chowdhury and Noble, 1996; Braithwaite et al., 2004; Denny et al., 2020). This relationship makes the evaluation of the formation process of dolomite more challenging.

The lower part of the third member and the upper part of the fourth member of the Eocene Shahejie Formation have thick organic-rich shales with substantial vertical and horizontal variations in lithofacies and reservoir characteristics (Zhu et al., 2004; Yuan et al., 2006). Dolomite and calcite are two main minerals and are widely distributed in organic-rich shales in the Dongying sag. Furthermore, the dolomite content in organic-rich shales reaches 95%. A few authors have interpreted the rhombohedral dolomite as authigenic precipitates formed during early diagenesis and burial through mineralogical and petrographic examinations in organic-rich shale in the Dongying sag (Liu et al., 2019). In the current research, the petrology, element composition, and Sr isotopes are integrated to investigate the origin of dolomite in organic shales from the Shahejie Formation of the Dongying Sag during burial diagenesis. The mean objectives of this study are as follows:

1) to identify the generation of the dolomites;
2) to clarify the potential source(s) for the dolomitization process in organic-rich shales;
3) to investigate the major dolomitization mechanism.

GEOLOGICAL SETTING

The Bohai Bay Basin (**Figure 1**), which developed on top of the Paleozoic North China Craton basement in eastern China, is a proliferous petroleum basin regarded as a significant target for shale oil (Ma et al., 2018; Luan et al., 2019). The basin has not experienced significant changes for the past 65 Ma (Jin et al., 2022). The Dongying sag is a Mesozoic-Cenozoic lacustrine half-graben rift-down warped basin lying in the southeastern Bohai Bay Basin (Cao et al., 2014; Ma et al., 2017). It covers an area of 5700 km^2 and is bounded to the east by the Qingtuozi Salient, to the south by the Luxi Uplift and Guangrao Salient, to the west by the Linfanjia and Gaoqing Salient, and to the north by the Chenjiazhuang-Binxian Salient (Guo et al., 2010; Luan et al., 2022). Due to the influences of the Tanlu fault, three predominant tectonic development stages have been experienced during sedimentary deposition, including an initial rifting stage, a sun-rifting stage and postrifting thermal subsidence (Liang et al., 2018).

From bottom to top, stratigraphic successions in the Dongying sag consist of the following formations: 1) the Paleogene Kongdian, Shahejie (Es), and Dongying; 2) the Neogene Guantao and Minghuazhen (Nm); and 3) the Quaternary Pingyuan (Qp). The Shahejie Formation can be divided into four intervals: Es1, Es2, Es3, and Es4. The Eocene Shahejie Formation was deposited with abundant algal organic matter inputs include dinoflagellates of the Defladrea, Senegalinium, Palacostomocysts species, and green algae (Bohaiensis, Pediastrum, and Botryococcus genera) (Geochemistry of petroleum systems in the Niuzhuang South Slope of Bohai Bay Basin—part 1: source rock characterization).

The upper Es4 and lower Es3 are the major layers for shale oil exploration (Feng et al., 2013). Due to the hot and dry paleoclimatic conditions and the broad, subsiding rift basin

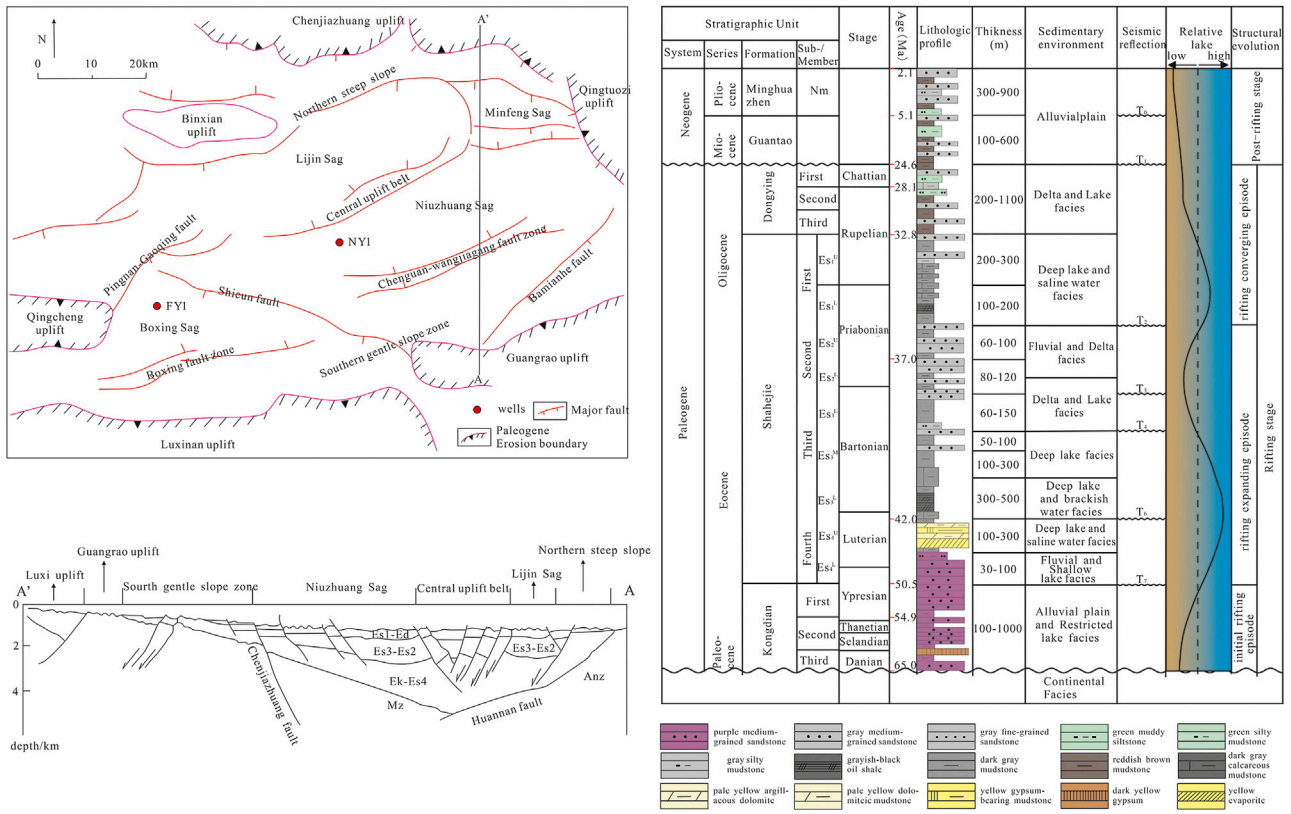

FIGURE 1 | Location, structural map and stratigraphic column of the Dongying Sag, modified after (He et al., 2017).

conditions with deep saltwater, a thick layer of gypsum and a set of organic-rich shales were deposited in Es4s. Previous studies have shown that seawater intrusion may have caused saltwater conditions and organic-rich shale deposition during this period (Liu et al., 2020). The early Es3, which was deposited in a stable lacustrine basin and humid paleo-climatic conditions, resulted in another set of organic-rich shales (Liang et al., 2017).

SAMPLING AND METHODOLOGY

A total of 42 samples were collected from the shale intervals of the NY1 and FY1 wells. All the samples were prepared as polished thin sections for detailed petrographic observation by polarizing microscopy and scanning electron microscopy (SEM).

Cathodoluminescence (CL) was performed under a microscope equipped with a CL8200- MK5 CL instrument at conditions of 17 kV and 600 μA.

Spot analyses of 42 major, trace, and rare earth elements in dolomite crystals were conducted by laser ablation–inductively coupled plasma–mass spectrometry (LA–ICP–MS) at Beijing Createch Testing International (Beijing, China) using an ESI NWR 193 nm excimer laser ablation system coupled to an Analytik Jena Plasma Quant mass spectrometer. The spot size and frequency of the laser were set to 35 mm and 10 Hz, respectively. All elements were calibrated against multiple synthetic reference glasses (NIST SRM 610, NIST SRM 612, BHVO-2G, BCR-2G, and BIR-1G). All the rare earth element (REE) values were normalized to the Post-Archean Australian Shale (PAAS) values, and Ce anomalies were used for calculations with the formulae of Bau and Dulski (1996).

The $^{87}Sr/^{86}Sr$ values of dolomites were analyzed with a Neptune Plus multicollector (MC)–ICP–MS equipped with a Resolution SE 193 nm excimer ArF laser ablation system at Beijing Createch Testing International (Beijing, China).

The bulk and clay X-ray diffraction (XRD) data of 168 samples and total organic carbon (TOC) contents of 146 samples were collected from Shengli Oilfield Company for basic mineral composition analysis.

RESULTS

Definition of Lithofacies

The shale samples from the Es4s and Es3x intervals in the NY1 and FY1 wells are composed of calcite (1–74%, average of 38.8%), quartz (1–62%, average of 23.9%), feldspar (1–35%, average of 3.6%), clay minerals (9–44%, average of 21.8%), dolomite (1–97%, average of 24.9%), pyrite (0–48%, average of 2.8%), and anhydrite (0–90%, average of 1.4%), with rich organic matter ranging from 0.15 to 12.28% (average of 4.1%). Five lithofacies, including light brown laminated calcareous shale,

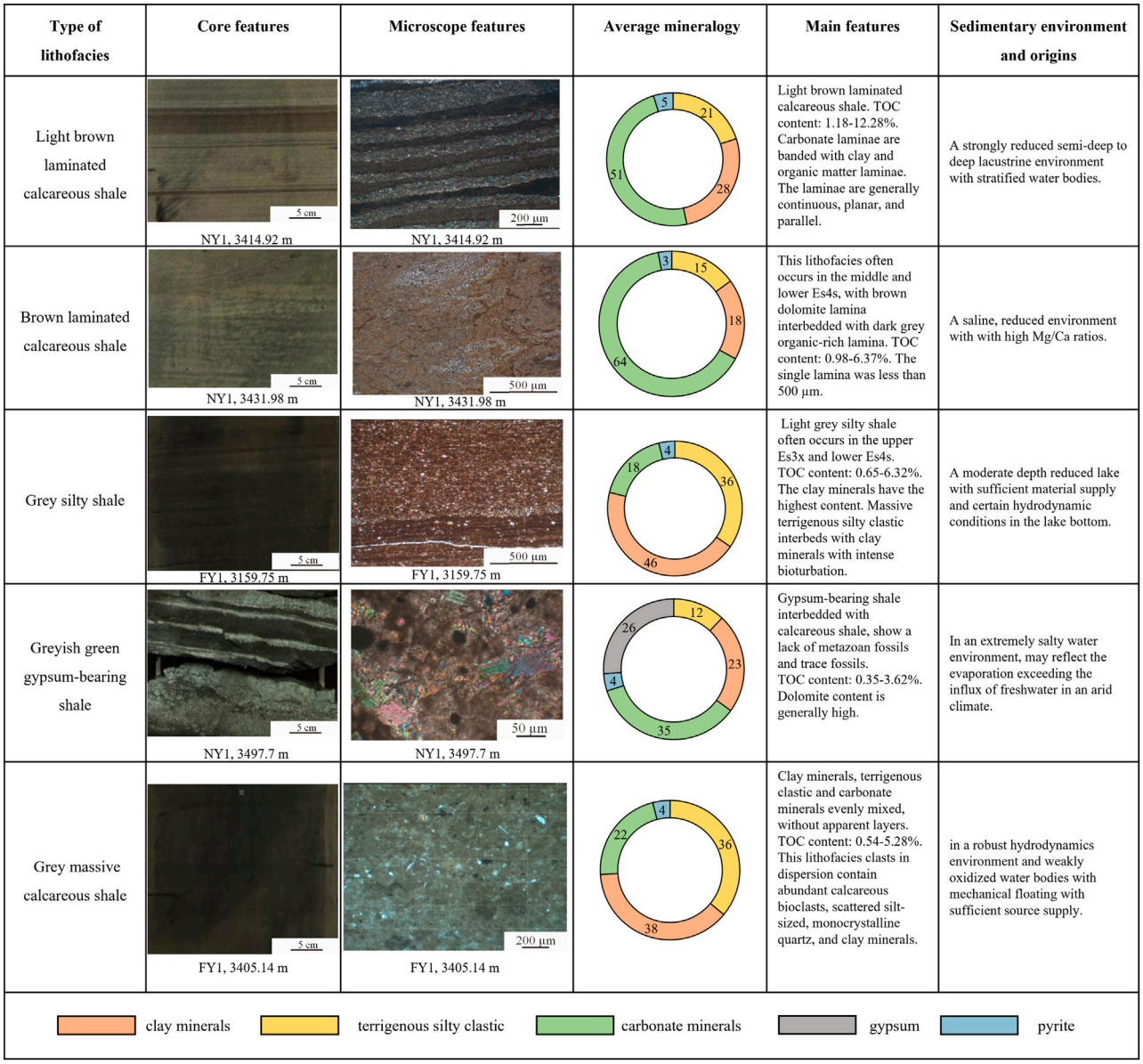

FIGURE 2 | Types and features of main lithofacies.

brown laminated calcareous shale, grey silty shale, greyish green gypsum-bearing shale, and grey massive calcareous shale, are defined according to the colour, structure, mineral composition, and TOC (**Figure 2**).

Dolomite Petrography

Petrographic examinations reveal four main generations of dolomite (Dol-1, Dol-2, Dol-3, and Dol-4). The investigated dolomite is mainly present in light brown laminated calcareous shale and brown laminated calcareous shale.

Dolomite 1 (Dol-1, 4–93%) occurs as scattered and/or laminated dolomicrite in all four lithofacies, showed the most abundant in the lower part of Es4s. It consists of a replacive micritic to near-micritic pervasive dolomite that ranges from 2 to 10 μm, is generally mimetic, and preserves sedimentary fabrics (**Figure 3A**). In addition, Dol-1 is usually tightly packed (nonporous) and has nonplanar mosaic micritic crystals with irregular intercrystallite boundaries and dull CL. Moreover, euhedral pyrites and pyrite framboids are often observed in the Dol-1-rich samples (**Figure 3E**).

Dolomite 2 (Dol-2, 2–27%) occurs as sub-to euhedral zoned rhombs (cloudy cores with clear rims) with a planar-e texture (**Figure 3B**), which are attributed to progressive dolomitization during burial and range from 20 to 100 μm (**Figure 3E**). Dol-2 is the most abundant in the upper part of Es3x and the middle part of Es4s, and it is especially less abundant in greyish green

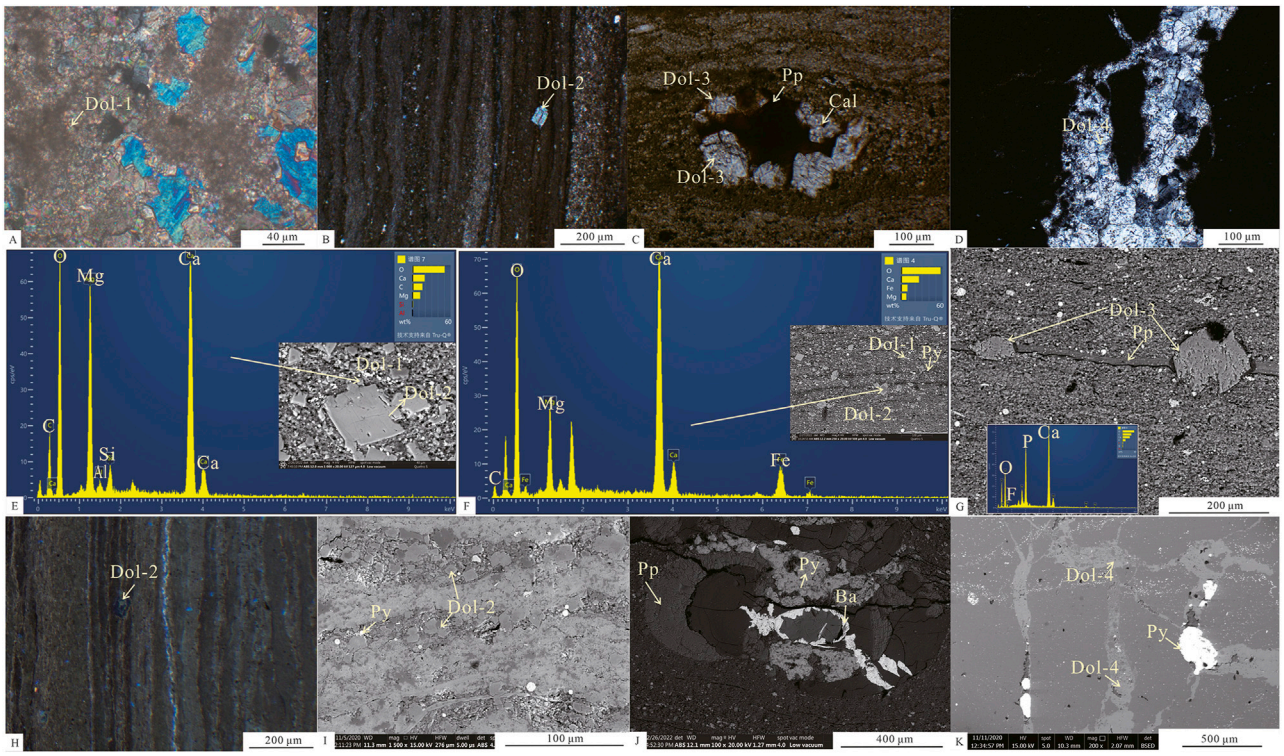

FIGURE 3 | Macroscopic and microscopic photographs of petrographic features of the investigated dolomites. **(A)** Tightly packed Dol-1 in greyish green gypsum-bearing shale, plane-polarized light, Well NY1, 3494.28 m. **(B)** Scattered Dol-2 in laminated calcareous shale, plane-polarized light, Well NY1, 3326.58 m. **(C)** Microscopic images of Dol-3, plane-polarized light, Well FY1, 3195.3 m. **(D)** Microscopic images of Dol-4, Well NY1, 3474.9 m **(E)** backscattered electron (BSE) image with energy-dispersive X-ray spectroscopy (EDS) spectrum of Dol-1, Well NY1, 3494.28 m **(F)** BSE image with EDS spectrum of Dol-2, Well FY1, 3211.53 m **(G)** BSE image with EDS spectrum of Dol-3, Well NY1, 3314.97 m **(H)** BSE image with EDS spectrum of Dol-1, Well NY1, 3494.28 m **(I)** BSE image of Dol-2, Well NY1, 3431.05 m **(J)** BSE image with EDS spectrum of barite, Well FY1, 3405.14 m **(K)** BSE image of Dol-4, Well NY1, 3474.9 m. Py-pyrite; Ba-barite.

gypsum-bearing shale in the lower part of Es4s (less than ca. 3%). Observations reveal that intercrystallite porosity is developed in Dol-2. Under fluorescence, Dol-2 shows zoned green/yellow autofluorescence (**Figure 3H**). Furthermore, euhedral pyrites and pyrite framboids show a syngenetic relationship with Dol-2.

Dolomite 3 (Dol-3) is not abundant. By qualitative evaluation, Dol-3 is less than ca. 1% per thin section and is usually scattered in organic-rich laminae in light brown laminated calcareous shale in lower Es3x (**Figure 3C**). In addition, some Dol-3 has synthetic relationships with barite and coalesced pyrite (**Figure 3J**). Dol-3 forms medium to coarse planar-s to nonplanar crystals (100–500 μm) with dull luminescence. Dol-3 crystals show undulate (sweeping) extinction similar to saddle dolomite, encased by phosphatic particles. In SEM images, these phosphatic particles are clearly remnantsof ostracods or algae (**Figure 3G**).

Dolomite 4 (Dol-4) postdates Dol-2 and consists of densely packed undeveloped unzoned crystals with irregular crystal boundaries (up to ca. ~5% volume) with coarser crystals than Dol-1 and Dol-2 (more than 500 μm in size) that appear relatively transparent under plane-polarized light (**Figure 3D**). This type of dolomite, which is observed only in a few abnormal pressures in calcareous shale samples, shows a syngenetic relationship with coalesced pyrite (**Figure 3K**). Under CL, Dol-4 exhibits a dull red luminescence. It shows corroded rims in fractures and has no sign of zoning or earlier fabric. As shown in **Figure 3K**, Dol-4 postdates the previous dolomite types and is the product of the latest diagenetic stage.

Occurrence of Dolomite in Shales

Observations found that dolomite has a high content in greyish green gypsum-bearing shale (5–98%, **Figure 4A**) and brown laminated calcareous shale (21–95%, **Figures 4B,C**). And Dol-1 and Dol-2 are often scattered and have less content (2%–21%, 4%–28%, respectively) in grey massive calcareous shale (**Figure 4D**) and grey silty shale (**Figure 4E**), mixed with scattered organic matter, clay minerals, calcite, and terrigenous debris (**Figures 4I,M**) with Dol-3 and Dol-4 rarely development.

Brown laminated calcareous shale, which brown dolomite lamina interbedded with dark grey organic-rich lamina (**Figures 4G,H**), with a single lamina was less than 500 μm. The dolomite lamina primary consisted of Dol-1, which is similar in texture to that found in modern settings where precipitation typically occurs in alkaline and saline waters with high Mg/Ca ratios (Last et al., 2012). Brown laminated calcareous shale was less developed, which was discontinuously developed vertically, with less than 40 cm thickness.

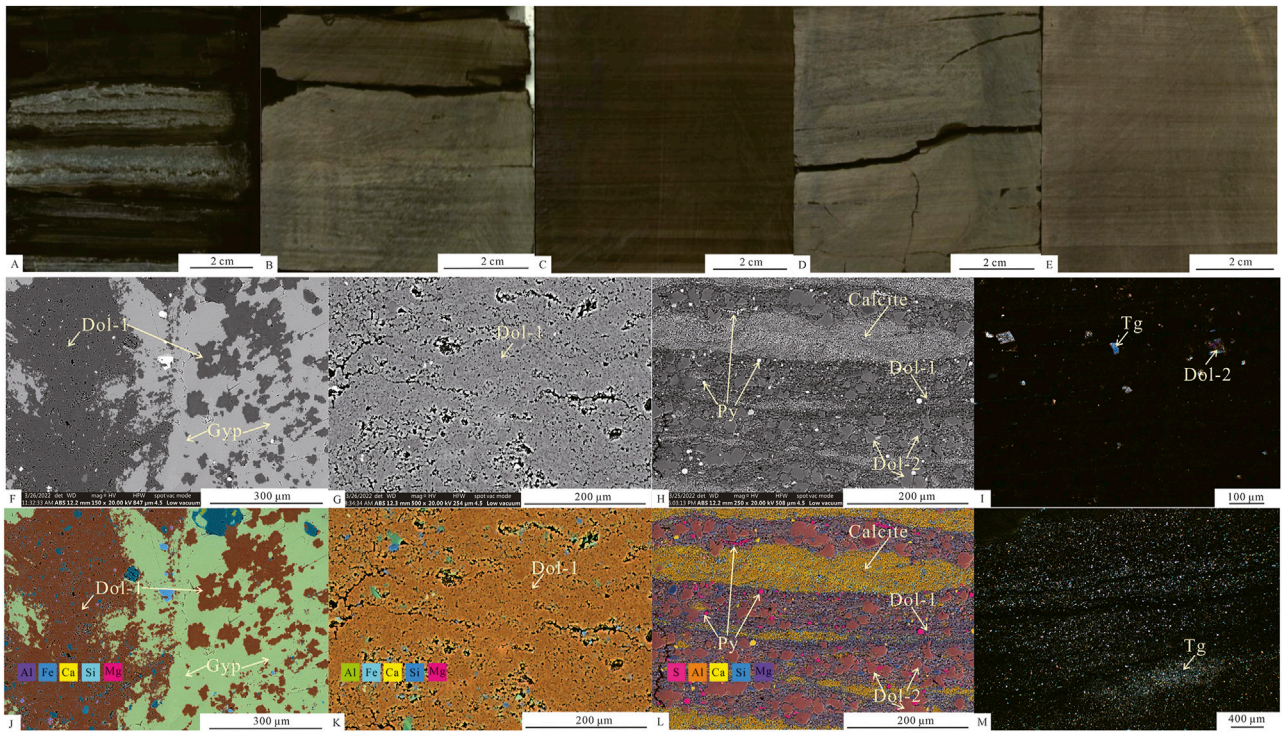

FIGURE 4 | Macroscopic and microscopic photographs of the investigated dolomites. **(A)** Greyish green gypsum-bearing shale, Well NY1, 3491.95 m. **(B)** Type I laminated calcareous shale, Well NY1, 3438.97 m. **(C)** Light brown laminated calcareous shale, Well FY1, 3361.44 m. **(D)** Grey massive calcareous shale, Well NY1, 3387.75 m. **(E)** Grey silty shale, Well NY1, 3468.65 m **(F)** BSE image of Dol-1 and gypsum in greyish green gypsum-bearing shale, Well NY1, 3491.95 m **(G)** BSE image of Dol-1 in brown laminated calcareous shale, Well NY1, 3438.97 m **(H)** BSE image of dolomite lamina in light brown laminated calcareous shale, Well FY1, 3361.44 m. **(I)** Microscopic image of grey massive calcareous shale, Well NY1, 3387.75 m **(J)** EDS mapping of Dol-1 and gypsum in greyish green gypsum-bearing shale, Well NY1, 3491.95 m **(K)** EDS mapping of Dol-1 in brown laminated calcareous shale, Well NY1, 3438.97 m **(L)** EDS mapping of dolomite lamina in light brown laminated calcareous shale, Well FY1, 3361.44 m. **(M)** Microscopic image of grey silty shale, Well NY1, 3468.65 m. Gyp-gypsum; Tg-terrigenous silty clastic; Py-pyrite.

Light brown laminated calcareous shale developed more frequently, forming continuous laminae to discontinuous lenses with alternating greyish and brown layers. The thickness of a single lamina is approximately 200 μm. The greyish layers are mainly Dol-2 and Dol-1 with clay minerals, terrigenous debris, and organic matter, while the brown layers are mainly composed of calcite (**Figures 4H,L**). Moreover, Dol-3 and Dol-4 are mainly observed in light brown laminated calcareous shale.

The enriched dolomite greyish green gypsum-bearing shale is composed of greyish-green and white layers, and the evaporative minerals are mixed with Dol-1 (**Figures 4F,J**).

Major and Trace Elements

Only two chemical compositional data points of Dol-1 are obtained due to its small mineral size. The geochemical compositions of the investigated dolomite are summarized in **Table 1**. Dol-1 has a lower CaO content (Dol-1 = 24.40 ± 2.45%, n = 2), while the other investigated dolomites have comparable CaO contents (Dol-2 = 37.50 ± 6.13%, n = 10; Dol-3 = 42.49 ± 9.72%, n = 6; Dol-4 = 45.59 ± 1.38%, n = 5). Among them, Dol-3 and Dol-4 are similar but are slightly higher than Dol-2. All four types of dolomites are comparable in MgO (Dol-1 = 18.56 ± 0.56%, n = 2; Dol-2 = 20.56 ± 5.08%, n = 10; Dol-3 = 20.56 ± 6.91%, n = 6; Dol-4 = 18.54 ± 0.76%, n = 5). Therefore, dolomites are mainly nonstoichiometric. From Dol-1 to Dol-4, the trace elements show progression, especially in Fe and Mn contents (**Figure 5A**), despite the general overlap in the elemental compositions. The Fe concentrations increase from 1598 ± 198 ppm in Dol-1 to 16861 ± 7926 ppm in Dol-2 to 18733 ± 8494 ppm to 22853 ± 1968 ppm in Dol-4. The Mn contents vary from 800 ± 66 ppm in Dol-1 to 5276 ± 2716 ppm in Dol-2 to 9098 ± 3800 ppm in Dol-4 to 3581 ± 271 ppm in Dol-4. The Sr concentrations decrease from approximately 1500 ppm in Dol-1 to approximately 500 ppm in Dol-4. Higher Sr contents than dolomite characterize calcite. The Mn content is similar to that of dolomite (**Figure 5B**).

Rare Earth Elements

Table 1 summarizes the statistics of the REE concentrations and the calculated Ce and Eu anomalies of the investigated samples from Es4s and Es3x. The mean ∑REE values of dolomites are the lowest in Dol-1 (40.48 ± 1.38 ppm, n = 2) and the highest in Dol-4 (155.91 ± 99.74 ppm, n = 6). Dol-2 and Dol-3 have moderate values (Dol-2 = 70.27 ± 14.92 ppm, n = 5; Dol-4 = 61.25 ± 28.06 ppm, n = 6). The variations in the REE concentrations of the investigated carbonate minerals are also indicated by their shale-normalized patterns (**Figure 6**).

TABLE 1 | CaO, MgO, Fe, Mn, Sr, REE, statistics of the investigated dolomites.

Phases		Na_2O (10^{-6})	CaO%	MgO%	Fe	Mn	Sr	La	Ce	Pr	Nd	Sm	Eu	Gd	Tb	Dy	Ho	Er	Tm	Yb	Lu	U	∑REE	δCe
Dol-1	n	2	2	2	2	2	2	2	2	2	2	2	2	2	2	2	2	2	2	2	2	2	2	2
	Mean	5085	24.4	15.6	1598	800	1461	8.256	17.371	1.803	7.512	1.434	0.310	1.214	0.174	1.046	0.213	0.561	0.080	0.507	0.070	1.540	40.6	1.03
	Max	6563	26.9	19.1	1796	867	1592	8.522	19.182	1.804	7.778	1.599	0.312	1.322	0.181	1.122	0.214	0.615	0.086	0.516	0.073	1.600	41.9	1.13
	Min	3606	22.0	18.0	1401	734	1329	7.991	15.560	1.802	7.246	1.270	0.309	1.107	0.167	0.970	0.211	0.507	0.075	0.498	0.066	1.481	39.2	0.94
Dol-2	n	10	10	10	10	10	10	10	10	10	10	10	10	10	10	10	10	10	10	10	10	10	10	10
	Mean	624	37.8	20.5	14519	4220	1531	13.311	28.692	3.246	13.447	2.417	0.614	2.114	0.350	2.131	0.436	1.147	0.158	1.026	0.147	1.195	66.5	1.03
	Max	1176	43.6	25.7	24788	7992	2476	29.587	56.903	6.068	23.576	4.703	1.698	5.074	0.896	5.747	1.167	2.925	0.392	2.223	0.259	3.734	131.2	1.13
	Min	225	31.4	15.5	8935	2560	803	6.434	14.064	1.382	5.098	0.837	0.202	0.697	0.135	0.804	0.168	0.435	0.058	0.402	0.061	0.161	31.5	0.93
Dol-3	n	6	6	6	6	6	6	6	6	6	6	6	6	6	6	6	6	6	6	6	6	6	6	6
	Mean	255	44.6	19.5	22786	9289	1529	9.605	31.979	4.077	17.293	3.264	0.918	2.823	0.438	2.759	0.542	1.326	0.153	0.776	0.107	0.431	100.6	1.17
	Max	652	52.2	27.5	27226.46	12889.40	2770	17.563	63.205	8.170	34.178	6.119	1.747	5.867	0.882	5.504	1.045	2.551	0.293	1.483	0.180	0.440	148.8	1.16
	Min	68	32.8	13.6	10239.20	5289	776	2.576	7.615	0.982	3.982	0.669	0.232	0.532	0.064	0.390	0.067	0.175	0.018	0.104	0.017	0.272	53.6	1.11
Dol-4	n	5	5	5	5	5	5	5	5	5	5	5	5	5	5	5	5	5	5	5	5	5	5	5
	Mean	255	45.5	18.6	23064	3527	588	9.854	20.251	3.246	18.495	5.291	1.417	7.142	0.903	4.083	0.649	1.254	0.130	0.618	0.086	0.037	73.4	0.86
	Max	483	46.6	19.3	24821	3851	724	11.210	25.964	4.163	22.557	6.454	1.716	8.188	1.087	4.870	0.740	1.388	0.148	0.693	0.110	0.066	89.3	0.87
	Min	369	44.6	17.8	20885	3311	491	7.729	16.524	2.693	14.680	4.332	1.142	6.059	0.724	3.288	0.529	1.019	0.116	0.532	0.069	0.009	59.4	0.83

The Dol-1, Dol-2, and Dol-3 patterns are very similar, although that of Dol-4 is different.

Calculations of the Ce and Eu anomalies (Bau and Dulski, 1996) show that Dol-4 has the lowest mean Ce anomaly (0.93 ± 0.08), whereas Dol-1 has the highest mean Ce anomaly (1.16 ± 0.06). The mean Ce anomalies of Dol-2 and Dol-1 are between the following end-member values: Dol-1 = 1.13 ± 0.09; Dol-2 = 1.01 ± 0.08. The Eu anomalies (**Figure 6**) range from 1.02 ± 0.11 in Dol-4 to 1.52 ± 0.28 in Dol-3.

Sr Isotopes

The $^{87}Sr/^{86}Sr$ ratios largely overlap in Dol-1 to Dol-4, with values of 0.71071–0.71133, 0.71080–0.71145, 0.71085–0.71131, and 0.71071–0.71083, respectively. The $^{87}Sr/^{86}Sr$ values of Dol-4 tend to be lower than those of the others (**Figure 7**).

DISCUSSION

Sedimentary Environmental Reconstruction During Dolomite Formation

The enrichment of Dol-1 in greyish green gypsum-bearing shale indicated that the formation of Dol-1 was continuously under shallow water, reducing evaporative and high-salinity environments in lower part of Es4s, with high ratios of Mg/Ca, which were thought to promote dolomitization.

The enrichment of dolomite in brown laminated calcareous shale was similar in texture to that found in modern settings where precipitation typically occurs in alkaline and saline waters, with high Mg/Ca ratios (Last et al., 2012). Such as in Pellet Lake and Milne Lake, laminated dolomites with small crystal sizes and poorly-defined faces are interpreted to form from lake water by rapid precipitation. And in lakes from Western Victoria, Australia, dolomites had been proved to precipitate as a result of 1) high salinity, 2) high Mg/Ca ratios, and 3) high alkalinity (Deckker and Last, 1988). These dolomite occur as similar to Dol-1. The flat parallel to wavy parallel laminae of dolomite in light brown laminated calcareous shale implies that the environment was stable for a period, and the alternation of greyish and brown layers indicates that the climate changed periodically on a small scale. The continuous regular alternation of greyish and brown layers is interpreted as a steady rhythm from seasonal changes. Previous studies show that algae's periodic thriving caused much calcite precipitation in the lake, and brown calcite lamina formed. In winter, greyish lamina was formed during intervals of algae productivity with a large number of organic accumulation (Zhao et al., 2019). In winter, algal activity declines, and the lake hydrodynamic conditions weaken. Organic-rich matter and debris tend to accumulate at the lake bottom. The occurrence of framboidal pyrite (**Figure 4H**) indicated a more anoxic environment. But the sporadical distribution of framboidal pyrite suggested the limited amount of SRB, which proved that the alkalinity of the anoxic environment is not elevated, and carbonate precipitation is inhibited continuously. Under such weak hydrodynamic conditions, the detrital and organic matter are accessibly preserved. Therefore, more minor dolomite precipitated, and organic matter accumulated among the debris.

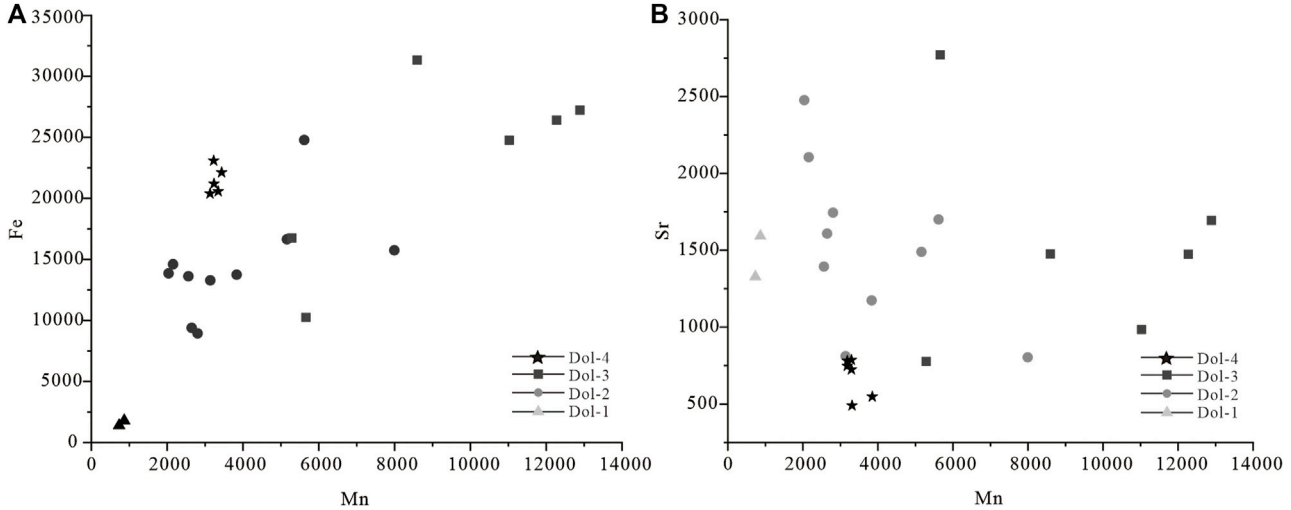

FIGURE 5 | Scatter diagrams of Mn vs. **(A)** Fe and **(B)** Sr for the investigated dolomites.

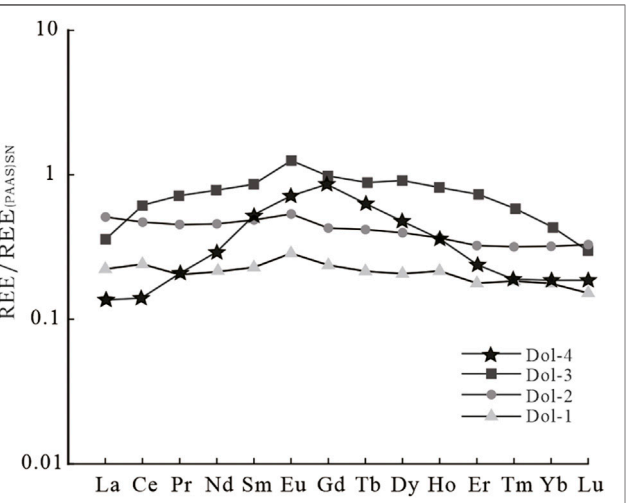

FIGURE 6 | Patterns of mean shale-normalized REE concentrations of the investigated dolomites.

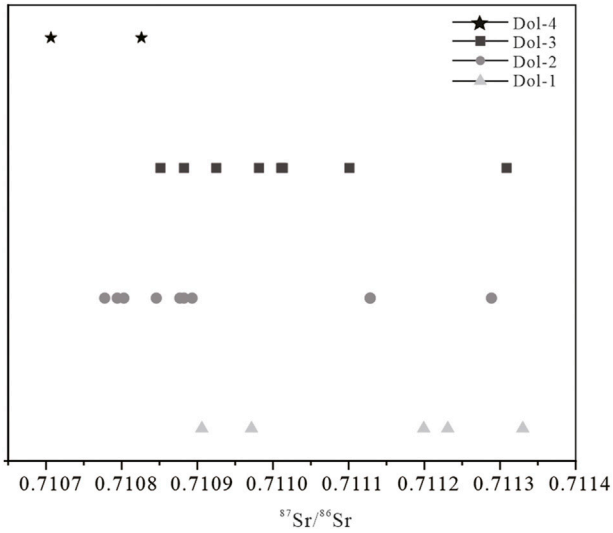

FIGURE 7 | $^{87}Sr/^{86}Sr$ values of the investigated dolomites.

Moreover, framboidal pyrite is distributed sporadically along with the sediment-water interface. So, the greyish layer formed.

VARIATIONS IN DOLOMITIZATION FLUIDS

Dolomite Petrography

As suggested by the petrographic characteristics of Dol-1, the nonluminescence of Dol-1 dolomite crystals under CL and its high Fe content indicate the widespread occurrence of Fe^{2+} (the main suppressor of luminescence in carbonate minerals) in dolomitizing fluids from which Dol-1 dolomites were formed (Machel, 1985; Savard et al., 1995; Perri and Tucker, 2007). The Dol-1 tends to be enriched in high-salinity, shallow water, reducing, and evaporative environments. That is, the parental fluid of this type of dolomite was most likely derived from the evaporation of water. Moreover, high Mg/Ca conditions favoured precipitation of dolomite. In addition, as gypsum forms, SO_4^{2-} can be consumed and reduce the inhibition of dolomite formation by sulfate ions. However, some Dol-1 has no syngenetic relationship with greyish green gypsum-bearing shale, indicating a lower salinity of dolomitizing fluid than gypsum precipitation (Lu and Meyers, 1998; Jones et al., 2000; Azomani et al., 2013; Rott and Qing, 2013; Olanipekun et al., 2014). Alternatively, Dol-1 could have precipitated from mixed evaporative meteoric waters (Azomani et al., 2013). Previous research has established that bacterial sulfate reduction (BSR) can

lower the kinetic barrier that prevents direct dolomite precipitation from magnesium-saturated brines at low temperatures, which would facilitate dolomite formation under such conditions (Vasconcelos et al., 1995; Vasconcelos and McKenzie, 1997; Van Lith et al., 2003; Petrash et al., 2017). Microscopic observations show the widespread occurrence of euhedral pyrites and pyrite framboids in the Dol-1-rich samples, suggesting that BSR may have been operative in reducing diagenetic fluids, which possibly promoted dolomite precipitation from mixed evaporative meteoric waters (Vasconcelos and McKenzie, 1997; Wacey et al., 2007; Bontognali et al., 2014). Additionally, BSR can consume SO_4^{2-} and release Mg^{2+} that provides Mg^{2+} for dolomitization.

Most Dol-2 crystals show cloudy cores with clear rims attributed to progressive dolomitization during burial that resulted in the replacement of precursor carbonate (cloudy cores) followed by later cementation as a clear rim during crystallization (Kırmacı, 2008; Rameil, 2008), with red rim and dull core CL images. The nonluminescence of the clear rims of Dol-2 dolomite crystals indicates the incorporation of Fe^{2+} during their further overgrowth in deeper burial realms (Machel, 1985; Savard et al., 1995). Moreover, the subhedral to euhedral crystals of Dol-2 suggest that they formed at low temperatures, likely lower than the critical roughening temperature for dolomites (50–60°C; Gregg and Sibley, 1984). While there are no clear remnant biological components revealed by SEM examination, the green/yellow autofluorescence of Dol-2 confirms the presence of diffuse organic matter, which points toward a biological association (Dupraz et al., 2004; Dupraz and Visscher, 2005; Perri and Tucker, 2007; Last et al., 2012). Dol-2 tends to accumulate in organic-rich laminae, indicating an organic matter-related origin.

In particular, Dol-3, which is encased by phosphatic particles and the remains of ostracods or algae, occurs with organic matter and is regarded as a potential microbial-related feature. The scattered residual phosphatic particles within Dol-3 indicate Dol-3 replacement of phosphatic particles (Liu et al., 2020). Results from earlier studies demonstrate that bacterial cells can, for example, serve as templates for the nucleation and growth of phosphatic particles in an oversaturated phosphate solution. In the study area, bacterial cells can also provide nucleation sites for dolomite crystals. The occurrence of phosphatic particle grains within organic matter may imply microbial degradation of organic matter, which releases phosphate to pore waters and promotes the reprecipitation of phosphate (Baturin and Kochenov, 2001). Furthermore, in contrast to Dol-1 and Dol-2, the coarser crystal sizes and nonplanar crystal surfaces with undulate (sweeping) extinction of Dol-3 suggest that it precipitated at higher temperatures during progressive burial (Gregg and Sibley, 1984; Gregg and Shelton, 1990), as indicated by the occurrence of enclosed barite and coalesced pyrite. Based on the burial history of the shale in Es4s and ES3x, the diagenetic temperatures of Dol-3 may exceed 100°C, considering the limited influence of hydrothermal activities in the Dongying sag (Song et al., 2009).

Fracture-filling Dol-4 (saddle dolomite) precipitated at high temperatures (over 100°C) during deep burial, as indicated by its undulate extinction (Gregg and Sibley, 1984). There might be some relationship with sulfate reduction, as indicated by the occurrence of enclosed coalesced pyrite in Dol-4 (Radke and Mathis, 1980). Pyrite filled the abnormal pressures related to the thermal evolution of organic matter, indicating that its formation had a close relationship with hydrothermal activities.

Major and Trace Elements

As shown in **Table 1**, the high Na content in Dol-1 is related to the high Mg/Ca fluid generated by strong syngenetic evaporation and concentration, and this kind of high-salinity fluid from strong evaporation can overcome the dynamic dolomitizing barrier to facilitate dolomite formation by alteration (Yang et al., 2021). The Ca concentrations of dolomite indicate that all types of dolomites are nonstoichiometric, showing that these nonstoichiometric dolomites are related to the formation of the rock-buffered diagenetic system (Warren, 2000) and lack sufficient fluid mobility and/or a relatively inadequate supply of Mg^{2+}. Previous studies show that lacustrine dolomites with an organogenic origin are mainly Ca-rich and finely crystalline (Armenteros, 2010). Thus, the high Ca contents of dolomites may be related to the carbonate-precipitating microbial consortium.

The high Sr contents of Dol-1 (Dol-1>550 ppm) support a sabkha or bacterial origin (Sánchez-Román et al., 2011; Azmy et al., 2013; Hou et al., 2016). Conventional distribution coefficients of dolomite (i.e., 0.015–0.06; Banner, 1995; Pedone and Dickson, 2000) and present-day Sr/Ca ratios of lake water (0.016–0.018) can reveal the origin and nature of their parent dolomitizing fluids in a particular diagenetic environment. The Sr/Ca molar ratio of the dolomitizing fluid can be calculated from the following equation:

$$D_{Sr} = \left[\left({}^{m}Sr/{}^{m}Ca \right)_{dol} / \left({}^{m}Sr/{}^{m}Ca \right)_{solution} \right]$$

Where ^{m}Sr and ^{m}Ca are the molar concentrations of Sr and Ca in dolomites, respectively. The calculated Sr levels of dolomite in the study are approximately 50–150 ppm. Thus, the ~1000 ppm average Sr concentration in the dolomite suggests that the mineral originated due to the replacement of aragonite. However, recent studies show that laboratory-precipitated microbial dolomite in a sulfate-rich culture demonstrates elevated Sr levels. The Sr concentration obtained from the experimental results is consistent with that of dolomite in the study area, which suggests that the origin of the dolomite in the study area is influenced by microbes.

Iron (Fe) and manganese (Mn) are regarded as reliable proxies of redox conditions (**Table 1**) because of their enrichment in carbonates in enhanced reducing conditions during progressive burial (Land, 1986), whereas they can also be influenced by the concentrations of these elements in the diagenetic fluid (Azomani et al., 2013; Olanipekun et al., 2014). The data show a clear trend in which the mean values of Fe and Mn increase with progressive burial from Dol-1 to Dol-2 to Dol-3. This trend suggests that the geochemical properties of dolomitization fluids are similar. The Sr isotope results support the former scenario.

Rare Earth Elements

Fifteen elements, ranging in atomic number from 57 (Lanthanum) to 71 (Lutetium) on the periodic table of elements, compose the rare earth element (REE) group, which is subdivided into three groups: 1) light rare earth elements (LREEs), from La to Nd; 2) medium rare earth elements (MREEs), from Sm to Dy; and 3) heavy rare earth elements (HREEs), from Ho to Lu. It has been demonstrated that the diagenesis of carbonates at low water/rock interaction ratios (insignificant recrystallization) does not significantly alter their REE compositions (Banner and Hanson, 1988; Webb and Kamber, 2000; Nothdurft et al., 2004; Webb et al., 2009). Therefore, REEs can provide significant information on chemical changes in diagenetic fluids, equilibrium in water-rock interactions, and even the properties of diagenetic fluids and redox conditions (Azmy et al., 2013; Azomani et al., 2013; Hou et al., 2016). All the REEs are trivalent, except for cerium (Ce) (Ce^{4+} in some redox-sensitive environments) and europium (Eu) (Eu^{2+} in hydrothermal waters), which have similar ionic radii. Their comparable distribution coefficients that are incorporated in carbonates provide clues about the geochemistry of the parent fluid (Sholkovitz et al., 1994; Shaojun and Mucci, 1995; Sholkovitz and Shen, 1995). REEs are stable and cannot be altered in diagenetic conditions with low water/rock interactions. Therefore, they can be regarded as good proxies of the nature and origin of diagenetic fluids and redox conditions.

The shale-normalized patterns of Dol-1, Dol-2, and Dol-3 are similar. Still, they exhibit insignificant differences, which strongly supports the suggested scenario of the same dolomitizing fluid in which its elemental composition varied slightly during dolomitization and excluded the involvement of magmatic fluids or fluids of other origins in dolomitization.

The Dol-1, Dol-2, and Dol-3 Ce/Ce* values are almost or approximately 1 (**Figure 6**), suggesting possible conditions for reduction (anoxic and dysoxic). However, the petrographic characteristics of Dol-1 support an early stage of dolomitization under surface or near-surface conditions. The slight enrichment in Ce indicates that the dolomitizing parent fluids mixed with fluids that progressively circulated with REE-rich, particularly Ce-rich, siliciclastic rocks in the basin, such as the cooccurring shales and sandstones, which changed its geochemical characteristics (Abanda and Hannigan, 2006).

However, the Ce/Ce* values of Dol-4 are different from those of other types of dolomite, which are lower than one. The petrographic characteristics of Dol-4 suggest its close relationship with the thermal evolution of organic matter, which causes this significant difference in Ce/Ce* compared to other types of dolomite. All samples have slight positive Eu/Eu* anomalies. These anomalies are usually associated with the dissolution of plagioclase feldspars in clastic rocks, such as sandstones (Bau et al., 2010). Moreover, the shale-normalized patterns of Dol-4 show a significant difference. The patterns are more similar to a bell-shaped curve compared to those of Dol-1, Dol-2, and Dol-3. This finding supports that the Dol-4 parent dolomitizing fluid had a different composition, possibly due to extensive circulation in the surrounding basinal rocks. This is consistent with the comparable REE mean values (**Table 1**) and their occurrence.

Sr Isotope

The Sr isotope values indicate a common source of dolomitization of the investigated dolomite. The Sr isotope values higher than those of seawater suggest that the deep burial conditions caused diagenetic fluids to circulate through clastic rocks, such as shale beds within the basin. The dolomitization resulted in a slight shift to more radiogenic values in the host carbonate.

Formation Mechanism of Dolomites in Lacustrine Shale

Dol-1: During the Es4s and Es3x periods, the Dongying sag was a lacustrine basin influenced by sea transgression, with warm, semiarid to arid climatic conditions. A sea transgression brought enough Mg^{2+} and increased the lake salinity. Moreover, this kind of setting was favourable for water evaporation and increased the salinity of water in the study area. The water salinity was elevated under such conditions, and the evaporites began precipitating (e.g., gypsum/anhydride). At that time, many Dol-1 crystals likely formed. In the deep part of the lacustrine basin, mixed evaporative meteoric waters were insufficient for the precipitation of evaporites (**Figure 8A**). Under both circumstances, BSR helped overcome the kinetic barrier of dolomite and promoted the precipitation of Dol-1 at a low temperature in Earth surface settings (Machel, 1985; Vasconcelos and McKenzie, 1997). Moreover, the initially deposited carbonate minerals provided nucleation sites for primaeval dolomite crystals, which was beneficial for dolomite precipitation. The heavy density of brines caused the brines to percolate to the deeper sediments, leading to extensive dolomitization. During this process, a minor number of Dol-1 crystals likely formed in organic-rich shales. At that time, the brines influenced BSR-mediated dolomite crystals, resetting their geochemical signatures. This process caused the BSR-mediated dolomite to have identical geochemical signatures to dolomite formed from evaporated water.

Dol 2: As suggested by Dol-1 petrological and geochemical characteristics, Dol-2 resulted from the recrystallization of the precursor Dol-1 during burial diagenesis and was influenced by the thermal evolution of organic matter. At such burial depths, the transformation of clay minerals during diagenesis can release magnesium ions that influence diagenetic fluid properties and the diagenetic microenvironment, thereby facilitating the process of dolomitization. Considering the mature stage of the organic matter, many organic acidic fluids and HS^- existed in these strata, which dissolved a small amount of calcite and provided adequate space for dolomitization. Furthermore, abundant Fe^{2+} in reductive lake environments combined with HS^- form sulfide and pyrite. The dolomitization process was also facilitated by sulfide dissolution, which explains the syngenetic relationship between Dol-2 and pyrite (**Figure 8B**).

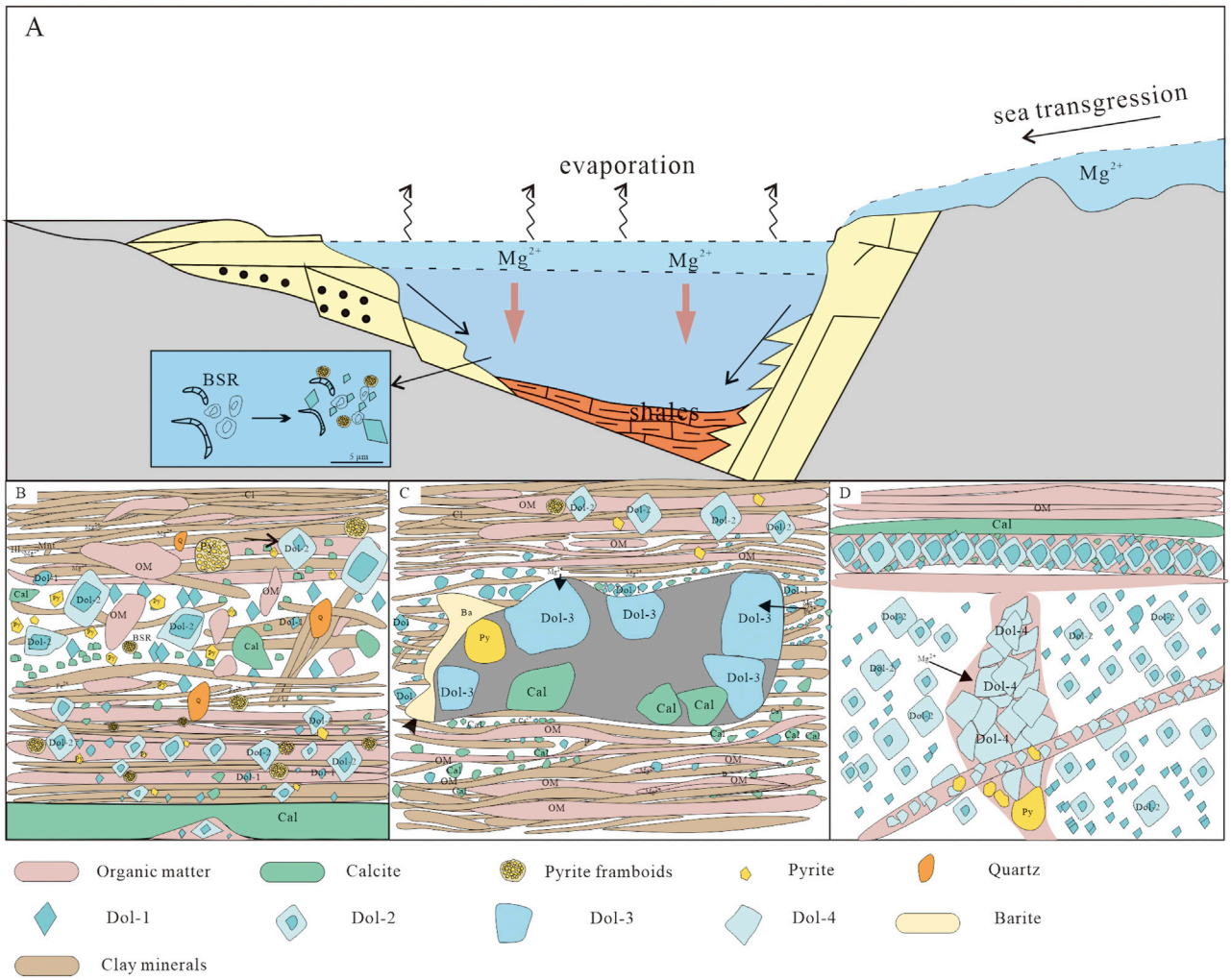

FIGURE 8 | Dolomitization mechanism of the investigated dolomite. Py-pyrite; Ba-barite; Cal-calcite; Dol-dolomite; Cl-clay minerals; Q-quartz; OM-organic matter.

Dol-3: Petrological and geochemical characteristics suggest that Dol-3 resulted from the intense recrystallization of previously formed dolomite. In winter, algal and Ostracoda died and deposited, forming a calcareous skeleton. At the early stage, bacteria inside calcified ostracods and algae provided nucleation sites for dolomite. The transformation of clay minerals and the dissolution of dissolved calcite and dolomite by organic acids provided enough Ca^{2+} and Mg^{2+} to the inside of calcified biological skeletons for dolomitization. Then, the geochemical characteristics of the former dolomite were resettled by early diagenetic fluid. Moreover, with the thermal evolution of organic matter, the inside temperature of calcified biological skeletons was high, which influenced the precipitation of Dol-3 (**Figure 8C**).

Dol-4: Several carbonate minerals were dissolved with the thermal evolution of organic matter, thereby supplying Mg^{2+} and Ca^{2+} to pore water. The transformation of clay minerals also provided Mg^{2+} and Ca^{2+} for dolomitization. Because of excessive pressure, a small number of abnormal pressures formed. This process released Mg^{2+}-rich pore water into the fractures, and then Dol-4 precipitated (**Figure 8D**).

CONCLUSION

Based on detailed field investigations and petrographic and geochemical analyses of the dolomite in the lacustrine organic-rich shale of the Shahejie Formation, Dongying sag, Bohai Bay Basin, the main conclusions are as follows:

1) Four types of dolomites, which represent episodic recrystallization, were classified based on crystal size and shape: (1) micritic dolomite (Dol-1), (2) euhedral dolomite (planar-e) (Dol-2), (3) anhedral dolomite (nonplanar) encased by phosphatic particles (Dol-3), and (4) fracture-filling anhedral dolomite (Dol-4).

2) Dol-1 formed from evaporated water or mixed evaporative meteoric waters with seawater provided by transgression during the early burial stage, possibly with microbial mediation (BSR).
3) Dol-2 resulted from recrystallization of the precursor Dol-1 during burial diagenesis and was influenced by the thermal evolution of organic matter.
4) Dol-3 likely resulted from intense recrystallization and was influenced by the thermal evolution of organic matter and bacterial activity.
5) Dol-4 precipitated from the hydrothermal fluid that resulted from the thermal evolution of organic matter, with extensive circulation in the surrounding basinal rocks.

DATA AVAILABILITY STATEMENT

The original contributions presented in the study are included in the article/Supplementary Material, further inquiries can be directed to the corresponding authors.

AUTHOR CONTRIBUTIONS

All authors listed have made a substantial, direct and intellectual contribution to the work, and approved it for publication.

FUNDING

This paper is supported by the National Natural Science Foundation of China (41972142; 42102153), China Postdoctoral Science Foundation (2021M693500), Specialized Fund for Shandong Postdoctoral Innovation Project (202103012), and the Fundamental Research Funds for the Central Universities (20CX06086A).

ACKNOWLEDGMENTS

We are grateful to Paulo Joaquim Nota from China University of Petroleum (East China) who modified the manuscript. We are indebted to Cunfei Ma from China University of Petroleum (East China) who collected and generously provided the shale samples.

REFERENCES

Abanda, P. A., and Hannigan, R. E. (2006). Effect of Diagenesis on Trace Element Partitioning in Shales. *Chem. Geol.* 230 (1-2), 42–59. doi:10.1016/j.chemgeo.2005.11.011

Armenteros, I. (2010). Chapter 2 Diagenesis of Carbonates in Continental Settings. *Deve. Sediment.* 62, 61–151. doi:10.1016/S0070-4571(09)06202-5

Azmy, K., Lavoie, D., Wang, Z., Brand, U., Al-Aasm, I., Jackson, S., et al. (2013). Magnesium-isotope and REE Compositions of Lower Ordovician Carbonates from Eastern Laurentia: Implications for the Origin of Dolomites and Limestones. *Chem. Geol.* 356, 64–75. doi:10.1016/j.chemgeo.2013.07.015

Azomani, E., Azmy, K., Blamey, N., Brand, U., and Al-Aasm, I. (2013). Origin of Lower Ordovician Dolomites in Eastern Laurentia: Controls on Porosity and Implications from Geochemistry. *Mar. Petroleum Geol.* 40, 99–114. doi:10.1016/j.marpetgeo.2012.10.007

Banner, J. L. (1995). Application of the Trace Element and Isotope Geochemistry of Strontium to Studies of Carbonate Diagenesis. *Sedimentology* 42 (5), 805–824. doi:10.1111/j.1365-3091.1995.tb00410.x

Baturin, G. N., and Kochenov, A. V. (2001). Uranium in Phosphorites. *Lithol. Min. Resour.* 36 (4), 303–321. doi:10.1023/A:1010406103447

Bau, M., Balan, S., Schmidt, K., and Koschinsky, A. (2010). Rare Earth Elements in Mussel Shells of the Mytilidae Family as Tracers for Hidden and Fossil High-Temperature Hydrothermal Systems. *Earth Planet. Sci. Lett.* 299 (3-4), 310–316. doi:10.1016/j.epsl.2010.09.011

Bau, M., and Dulski, P. (1996). Distribution of Yttrium and Rare-Earth Elements in the Penge and Kuruman Iron-Formations, Transvaal Supergroup, South Africa. *Precambrian Res.* 79 (1-2), 37–55. doi:10.1016/j.precamres.2018.07.01410.1016/0301-9268(95)00087-9

Bontognali, T. R. R., McKenzie, J. A., Warthmann, R. J., and Vasconcelos, C. (2014). Microbially Influenced Formation of Mg-Calcite and Ca-Dolomite in the Presence of Exopolymeric Substances Produced by Sulphate-Reducing Bacteria. *Terra nova.* 26 (1), 72–77. doi:10.1111/ter.12072

Bontognali, T. R. R., Vasconcelos, C., Warthmann, R. J., Bernasconi, S. M., Dupraz, C., Strohmenger, C. J., et al. (2010). Dolomite Formation within Microbial Mats in the Coastal Sabkha of Abu Dhabi (United Arab Emirates). *Sedimentology* 57 (3), 824–844. doi:10.1111/j.1365-3091.2009.01121.x

Bontognali, T. R. R., Vasconcelos, C., Warthmann, R. J., Dupraz, C., Bernasconi, S. M., and McKenzie, J. A. (2008). Microbes Produce Nanobacteria-like Structures, Avoiding Cell Entombment. *Geol* 36 (8), 663–666. doi:10.1130/G24755A.1

Braithwaite, C. J. R., Rizzi, G., and Darke, G. (2004). The Geometry and Petrogenesis of Dolomite Hydrocarbon Reservoirs: Introduction. *Geol. Soc. Lond. Spec. Publ.* 235 (1), 1–6. doi:10.1144/GSL.SP.2004.23510.1144/gsl.sp.2004.235.01.01

Radke, B. M., and Mathis, R. L. (1980). On the Formation and Occurrence of Saddle Dolomite. *Sepm Jsr* 50 (4), 1149–1168. doi:10.1306/212F7B9E-2B24-11D7-8648000102C1865D

Burns, S. J., Mckenzie, J. A., and Vasconcelos, C. (2010). Dolomite Formation and Biogeochemical Cycles in the Phanerozoic. *Sedimentology* 47 (s1), 49–61. doi:10.1016/j.chemgeo.2013.10.012

Cao, Y., Yuan, G., Li, X., Wang, Y., Xi, K., Wang, X., et al. (2014). Characteristics and Origin of Abnormally High Porosity Zones in Buried Paleogene Clastic Reservoirs in the Shengtuo Area, Dongying Sag, East China. *Pet. Sci.* 11 (3), 346–362. doi:10.1007/s12182-014-0349-y

Chowdhury, A. H., and Noble, J. P. A. (1996). Origin, Distribution and Significance of Carbonate Cements in the Albert Formation Reservoir Sandstones, New Brunswick, Canada. *Mar. Petroleum Geol.* 13 (7), 837–846. doi:10.1016/0264-8172(96)00002-5

Vasconcelos, C., and McKenzie, J. A. (1997). Microbial mediation of modern dolomite precipitation and diagenesis under anoxic conditions (Lagoa Vermelha, Rio de Janeiro, Brazil). *Sepm Jsr* 67 (3), 378–390. doi:10.1306/D4268577-2B26-11D7-8648000102C1865D

Davies, G. R. (1979). *Dolomite Reservoir Rocks: Processes, Controls, Porosity Development*. American Association of Petroleum Geologists.

Deckker, P. D., and Last, W. M. (1988). Modern Dolomite Deposition in Continental, Saline Lakes, Western Victoria, Australia. *Geol* 16 (1), 292–332. doi:10.1130/0091-7613(1988)016<0029:MDDICS>2.3.CO10.1130/0091-7613(1988)016<0029:mddics>2.3.co;2

Denny, A. C., Orland, I. J., and Valley, J. W. (2020). Regionally Correlated Oxygen and Carbon Isotope Zonation in Diagenetic Carbonates of the Bakken Formation. *Chem. Geol.* 531, 119327. doi:10.1016/j.chemgeo.2019.119327

Diloreto, Z. A., Garg, S., Bontognali, T. R. R., Dittrich, M. E. C., Fones, E. M., et al. (2020). Modern Dolomite Formation Caused by Seasonal Cycling of Oxygenic Phototrophs and Anoxygenic Phototrophs in a Hypersaline sabkhaAn Ecological Perspective on Dolomite Formation in Great Salt Lake, Utah. *Sci. Rep.Front. Earth Sci.* 1124, 41701–41713. doi:10.1038/s41598-021-83676-1Dunham10.3389/feart.2020.00024

Dupraz, C., Visscher, P. T., Baumgartner, L. K., and Reid, R. P. (2004). Microbe-mineral Interactions: Early Carbonate Precipitation in a Hypersaline Lake (Eleuthera Island, Bahamas). *Sedimentology* 51 (4), 745–765. doi:10.1111/j.1365-3091.2004.00649.x

Dupraz, C., and Visscher, P. T. (2005). Microbial Lithification in Marine Stromatolites and Hypersaline Mats. *Trends Microbiol.* 13 (9), 429–438. doi:10.1016/j.tim.2005.07.008

Feng, Y., Li, S., and Lu, Y. (2013). Sequence Stratigraphy and Architectural Variability in Late Eocene Lacustrine Strata of the Dongying Depression, Bohai Bay Basin, Eastern China. *Sediment. Geol.* 295, 1–26. doi:10.1016/j.sedgeo.2013.07.004

Guo, X., He, S., Liu, K., Song, G., Wang, X., and Shi, Z. (2010). Oil Generation as the Dominant Overpressure Mechanism in the Cenozoic Dongying Depression, Bohai Bay Basin, China. *Bulletin* 94 (12), 1859–1881. doi:10.1306/05191009179

He, J., Ding, W., Jiang, Z., Jiu, K., Li, A., and Sun, Y. (2017). Mineralogical and Chemical Distribution of the Es3L Oil Shale in the Jiyang Depression, Bohai Bay Basin (E China): Implications for Paleoenvironmental Reconstruction and Organic Matter Accumulation. *Mar. Petroleum Geol.* 81, 196–219. doi:10.1016/j.marpetgeo.2017.01.007

Hou, Y., Azmy, K., Berra, F., Jadoul, F., Blamey, N. J. F., Gleeson, S. A., et al. (2016). Origin of the Breno and Esino Dolomites in the Western Southern Alps (Italy): Implications for a Volcanic Influence. *Mar. Petroleum Geol.* 69, 38–52. doi:10.1016/j.marpetgeo.2015.10.010

Hsu, K. J. (1966). Origin of Dolomite in Sedimentary Sequences: A Critical Analysis. *Mineral. Deposita* 1 (2), 133–138. doi:10.1007/bf00206182

Irwin, H., Curtis, C., and Coleman, M. (1977). Isotopic Evidence for Source of Diagenetic Carbonates Formed during Burial of Organic-Rich Sediments. *Nature* 269 (5625), 209–213. doi:10.1038/269209a0

Banner, J. L., and Hanson, G. N., (1988). Rare Earth Element and Nd Isotopic Variations in Regionally Extensive Dolomites from the Burlington-Keokuk Formation (Mississippian): Implications for Ree Mobility during Carbonate Diagenesis. *Sepm Jsr* 58 (3), 415–432. doi:10.1306/212F8DAA-2B24-11D7-8648000102C1865D

Gregg, J. M, and Sibley, D. F. (1984). Epigenetic Dolomitization and the Origin of Xenotopic Dolomite Texture. *Sepm Jsr* 54 (3), 908–931. doi:10.1306/212F8535-2B24-11D7-8648000102C1865D

Gregg, J. M., and Shelton, K. L. (1990). Dolomitization and Dolomite Neomorphism in the Back Reef Facies of the Bonneterre and Davis Formations (Cambrian), Southeastern Missouri. *Sepm Jsr* 60 (4), 549–562. doi:10.1306/212F91E2-2B24-11D7-8648000102C1865D

Jin, S., Liu, S., Li, Z., Chen, A., and Ma, C. (2022). Astrochronology of a Middle Eocene Lacustrine Sequence and Sedimentary Noise Modeling of Lake-Level Changes in Dongying Depression, Bohai Bay Basin. *Palaeogeogr. Palaeoclimatol. Palaeoecol.* 585, 110740. doi:10.1016/j.palaeo.2021.110740

Jones, G., Whitaker, F., Smart, P., and Sanford, W. (2000). Numerical Modelling of Geothermal and Reflux Circulation in Enewetak Atoll: Implications for Dolomitization. *J. Geochem. Explor.* 69-70, 71–75. doi:10.1016/S0375-6742(00)00010-8

Kırmacı, M. Z. (2008). Dolomitization of the Late Cretaceous-Paleocene Platform Carbonates, Gölköy (Ordu), Eastern Pontides, NE Turkey. *Sediment. Geol.* 203 (3-4), 289–306. doi:10.1016/j.sedgeo.2007.12.009

Land, L. (1986). Environments of Limestone and Dolomite Diagenesis: Some Geochemical Considerations. *Carbonate Depositional Environ. Mod. Anc.* 5, 1.

Land, L. ST. (1992). The Dolomite Problem: Stable and Radiogenic Isotope Clues. *Lecture Notes in Earth Sciences*, 43. 49–68.doi:10.1007/bfb0009861

Last, F. M., Last, W. M., and Halden, N. M. (2012). Modern and Late Holocene Dolomite Formation: Manito Lake, Saskatchewan, Canada. *Sediment. Geol.* 281, 222–237. doi:10.1016/j.sedgeo.2012.09.012

Li, G., Lin, C., Dong, C., Ma, P., Du, X., Jiang, L., et al. (2022). Sequence Stratigraphy, Depositional Environment and Associated Lithofacies of Lacustrine Shale: A Case from the Upper Fourth Member of Shahejie Formation, Dongying Depression, Bohai Bay Basin. *Front. Earth Sci.* 10, 906987. doi:10.3389/feart.2022.906987

Liang, C., Cao, Y., Jiang, Z., Wu, J., Guoqi, S., and Wang, Y. (2017). Shale Oil Potential of Lacustrine Black Shale in the Eocene Dongying Depression: Implications for Geochemistry and Reservoir Characteristics. *Bulletin* 101 (11), 1835–1858. doi:10.1306/01251715249

Liang, C., Cao, Y., Liu, K., Jiang, Z., Wu, J., and Hao, F. (2018). Diagenetic Variation at the Lamina Scale in Lacustrine Organic-Rich Shales: Implications for Hydrocarbon Migration and Accumulation. *Geochimica Cosmochimica Acta* 229, 112–128. doi:10.1016/j.gca.2018.03.017

Liu, D., Li, Z., Jiang, Z., Zhang, C., Zhang, Z., Wang, J., et al. (2019a). Impact of Laminae on Pore Structures of Lacustrine Shales in the Southern Songliao Basin, NE China. *J. Asian Earth Sci.* 182, 103935. doi:10.1016/j.jseaes.2019.103935

Liu, H., Zhang, S., Song, G., Xuejun, W., Teng, J., Wang, M., et al. (2019b). Effect of Shale Diagenesis on Pores and Storage Capacity in the Paleogene Shahejie Formation, Dongying Depression, Bohai Bay Basin, East China. *Mar. Petroleum Geol.* 103, 738–752. doi:10.1016/j.marpetgeo.2019.01.002

Liu, S., Jiang, Z., He, Y., Dou, L., Yang, Y., Li, Y., et al. (2020). Geomorphology, Lithofacies and Sedimentary Environment of Lacustrine Carbonates in the Eocene Dongying Depression, Bohai Bay Basin, China. *Mar. Petroleum Geol.* 113, 104125. doi:10.1016/j.marpetgeo.2019.104125

Lu, F. H., and Meyers, W. J. (1998). Massive Dolomitization of a Late Miocene Carbonate Platform: a Case of Mixed Evaporative Brines with Meteoric Water, Nijar, Spain. *Sedimentology* 45 (2), 263–277. doi:10.1046/j.1365-3091.1998.0142e.x

Luan, G., Azmy, K., Dong, C., Lin, C., Ren, L., and Shi, C. (2022). Carbonate Cements in Eocene Turbidite Sandstones, Dongying Depression, Bohai Bay Basin: Origin, Distribution, and Effect on Reservoir Properties. *Bulletin* 106 (1), 209–240. doi:10.1306/07202120012

Luan, G., Dong, C., Azmy, K., Lin, C., Ma, C., Ren, L., et al. (2019). Origin of Bedding-Parallel Fibrous Calcite Veins in Lacustrine Black Shale: A Case Study from Dongying Depression, Bohai Bay Basin. *Mar. Petroleum Geol.* 102, 873–885. doi:10.1016/j.marpetgeo.2019.01.010

Ma, C., Dong, C., Elsworth, D., Wang, Q., Huang, Z., Liu, H., et al. (2020). Insights from Electron Backscatter Diffraction into the Origin of Fibrous Calcite Veins in Organic-Rich Shale from Lower Es3 to Upper Es4, Jiyang Depression, China. *Mar. Petroleum Geol.* 113, 104131. doi:10.1016/j.marpetgeo.2019.104131

Ma, P., Lin, C., Jahren, J., Dong, C., Ren, L., and Hellevang, H. (2021). Cyclic Zoning in Authigenic Saddle Dolomite-Ankerite: Indications of a Complex Interplay between Fault-Rupturing and Diagenetic Alteration. *Chem. Geol.* 559, 119831. doi:10.1016/j.chemgeo.2020.119831

Ma, P., Lin, C., Zhang, S., Dong, C., Zhao, Y., Dong, D., et al. (2018). Diagenetic History and Reservoir Quality of Tight Sandstones: A Case Study from Shiqianfeng Sandstones in Upper Permian of Dongpu Depression, Bohai Bay Basin, Eastern China. *Mar. Petroleum Geol.* 89, 280–299. doi:10.1016/j.marpetgeo.2017.09.029

Ma, Y., Fan, M., Lu, Y., Liu, H., Hao, Y., Xie, Z., et al. (2017). Middle Eocene Paleohydrology of the Dongying Depression in Eastern China from Sedimentological and Geochemical Signatures of Lacustrine Mudstone. *Palaeogeogr. Palaeoclimatol. Palaeoecol.* 479, 16–33. doi:10.1016/j.palaeo.2017.04.011

Machel, H.-G. (1985). Cathodoluminescence in Calcite and Dolomite and its Chemical Interpretation. *Geosci. Can.* 12, 271–301.

Machel, H. G. (2004). Concepts and Models of Dolomitization: a Critical Reappraisal. *Geol. Soc. Lond. Spec. Publ.* 235 (1), 7–63. doi:10.1144/GSL.SP.2004.235.01.02

Mazzullo, S. J. (2000). Organogenic Dolomitization in Peritidal to Deep-Sea Sediments. *J. Sediment. Res.* 70 (1), 10–23. doi:10.1306/2DC408F9-0E47-11D7-8643000102C1865D

Morrow, D. W. (1982). Diagenesis. Dolomite - Part I: The Chemistry of Dolomitization and Dolomite Precipitation. *Geosci. Can.* 9, 3–99.

Nothdurft, L. D., Webb, G. E., and Kamber, B. S. (2004). Rare Earth Element Geochemistry of Late Devonian Reefal Carbonates, Canning Basin, Western Australia: Confirmation of a Seawater REE Proxy in Ancient Limestones. *Geochimica Cosmochimica Acta* 68 (2), 263–283. doi:10.1016/S0016-7037(03)00422-8

Olanipekun, B.-J., Azmy, K., and Brand, U. (2014). Dolomites of the Boat Harbour Formation in the Northern Peninsula, Western Newfoundland, Canada: Implications for Dolomitization History and Porosity Control. *Bulletin* 98 (4), 765–791. doi:10.1306/08281312141

Pedone, V. A., and Dickson, J. A. D. (2000). Replacement of Aragonite by Quasi-Rhombohedral Dolomite in a Late Pleistocene Tufa Mound, Great Salt Lake, Utah, U.S.A. *J. Sediment. Res.* 70 (5), 1152–1159. doi:10.1306/041200701152

Perri, E., and Tucker, M. (2007). Bacterial Fossils and Microbial Dolomite in Triassic Stromatolites. *Geol* 35 (3), 207–210. doi:10.1130/G23354A.1

Petrash, D. A., Bialik, O. M., Bontognali, T. R. R., Vasconcelos, C., Roberts, J. A., McKenzie, J. A., et al. (2017). Microbially Catalyzed Dolomite Formation: From

Near-Surface to Burial. *Earth-Science Rev.* 171, 558–582. doi:10.1016/j.earscirev.2017.06.015

Pu, X., Zhou, L., Han, W., Zhou, J., Wang, W., Zhang, W., et al. (2016). Geologic Features of Fine-Grained Facies Sedimentation and Tight Oil Exploration: A Case from the Second Member of Paleogene Kongdian Formation of Cangdong Sag, Bohai Bay Basin. *Petroleum Explor. Dev.* 43 (1), 26–35. doi:10.1016/S1876-3804(16)30003-9

Rameil, N. (2008). Early Diagenetic Dolomitization and Dedolomitization of Late Jurassic and Earliest Cretaceous Platform Carbonates: a Case Study from the Jura Mountains (NW Switzerland, E France). *Sediment. Geol.* 212 (1-4), 70–85. doi:10.1016/j.sedgeo.2008.10.004

Rott, C. M., and Qing, H. (2013). Early Dolomitization and Recrystallization in Shallow Marine Carbonates, Mississippian Alida Beds, Williston Basin (Canada): Evidence from Petrography and Isotope Geochemistry. *J. Sediment. Res.* 83 (11), 928–941. doi:10.2110/jsr.2013.73

Sánchez-Román, M., Romanek, C. S., Fernández-Remolar, D. C., Sánchez-Navas, A., McKenzie, J. A., Pibernat, R. A., et al. (2011). Aerobic Biomineralization of Mg-Rich Carbonates: Implications for Natural Environments. *Chem. Geol.* 281 (3-4), 143–150. doi:10.1016/j.chemgeo.2010.11.020

Savard, M. M., Veizer, J., and Hinton, R. (1995). Cathodoluminescene at Low Fe and Mn Concentrations; a SIMS Study of Zones in Natural Calcites. *J. Sediment. Res.* 65 (1a), 208–213. doi:10.1306/D4268072-2B26-11D7-8648000102C1865D

Seewald, J. S. (2003). Organic-inorganic Interactions in Petroleum-Producing Sedimentary Basins. *Nature* 426 (6964), 327–333. doi:10.1038/nature02132

Shaojun, Z., Mucci, A. G., and Stille, P. (1995). Partitioning of Rare Earth Elements (REEs) between Calcite and Seawater Solutions at 25°C and 1 Atm, and High Dissolved REE concentrationsDiagenetic Constraints on the Use of Cerium Anomalies as Palaeoseawater Redox Proxies: an Isotopic and REE Study of Cambrian Phosphorites. *Geochim. Cosmochim. Acta.Chemical Geol.* 59175 (31-2), 44329–45348. doi:10.1016/0016-7037(94)00381-UShields10.1016/S0009-2541(00)00362-4

Sholkovitz, E. R., Landing, W. M., and Lewis, B. L. (1994). Ocean Particle Chemistry: the Fractionation of Rare Earth Elements between Suspended Particles and Seawater. *Geochimica Cosmochimica Acta* 58 (6), 1567–1579. doi:10.1016/0016-7037(94)90559-2

Sholkovitz, E., and Shen, G. T. (1995). The Incorporation of Rare Earth Elements in Modern Coral. *Geochimica Cosmochimica Acta* 59 (13), 2749–2756. doi:10.1016/0016-7037(95)00170-5

Shukla, V., and Baker, P. A. (1988). *Sedimentology and Geochemistry of Dolostones, Sedimentology and Geochemistry of Dolostones : Based on a Symposium*. California: Society of Economic Paleontologists and Mineralogists.

Song, G., Jiang, Y., Liu, H., and Cai, D. (2009). Pooling History of Cracked Gas in Middle-Deep Reservoirs in Lijin-Minfeng Areas of the Dongying Sag. *Nat. Gas. Ind.* 29 (4), 14–17.

Tang, Y., Cao, J., He, W.-J., Guo, X.-G., Zhao, K.-B., and Li, W.-W. (2021). Discovery of Shale Oil in Alkaline Lacustrine Basins: The Late Paleozoic Fengcheng Formation, Mahu Sag, Junggar Basin, China. *Petroleum Sci.* 18 (5), 1281–1293. doi:10.1016/j.petsci.2021.04.001

Tian, S., Bowen, L., Liu, B., Zeng, F., Xue, H., Erastova, V., et al. (2021). A Method for Automatic Shale Porosity Quantification Using an Edge-Threshold Automatic Processing (ETAP) Technique. *Fuel* 304, 121319. doi:10.1016/j.fuel.2021.121319

Van Lith, Y., Warthmann, R., Vasconcelos, C., and Mckenzie, J. A. (2003). Sulphate-reducing Bacteria Induce Low-Temperature Ca-Dolomite and High Mg-Calcite Formation. *Geobiology* 1 (1), 71–79. doi:10.1046/j.1472-4669.2003.00003.x

Vasconcelos, C., McKenzie, J. A., Bernasconi, S., Grujic, D., and Tiens, A. J. (1995). Microbial Mediation as a Possible Mechanism for Natural Dolomite Formation at Low Temperatures. *Nature* 377 (6546), 220–222. doi:10.1038/377220a0

Vasconcelos, C., Warthmann, R., McKenzie, J. A., Visscher, P. T., Bittermann, A. G., and van Lith, Y. (2006). Lithifying Microbial Mats in Lagoa Vermelha, Brazil: Modern Precambrian Relics? *Sediment. Geol.* 185 (3-4), 175–183. doi:10.1016/j.sedgeo.2005.12.022

Vengosh, A., Jackson, R. B., Warner, N., Darrah, T. H., and Kondash, A. (2014). A Critical Review of the Risks to Water Resources from Unconventional Shale Gas Development and Hydraulic Fracturing in the United States. *Environ. Sci. Technol.* 48 (15), 8334–8348. doi:10.1021/es405118y

Wacey, D., Wright, D. T., and Boyce, A. J. (2007). A Stable Isotope Study of Microbial Dolomite Formation in the Coorong Region, South Australia. *Chem. Geol.* 244 (1-2), 155–174. doi:10.1016/j.chemgeo.2007.06.032

Warren, J. (2000). Dolomite: Occurrence, Evolution and Economically Important Associations. *Earth Sci. Rev.* 52 (1-3), 1–81. doi:10.1016/S0012-8252(00)00022-2

Webb, G. E., and Kamber, B. S. (2000). Rare Earth Elements in Holocene Reefal Microbialites: a New Shallow Seawater Proxy. *Geochimica Cosmochimica Acta* 64 (9), 1557–1565. doi:10.1016/S0016-7037(99)00400-7

Webb, G. E., Nothdurft, L. D., Kamber, B. S., Kloprogge, J. T., and Zhao, J.-X. (2009). Rare Earth Element Geochemistry of Scleractinian Coral Skeleton during Meteoric Diagenesis: a Sequence through Neomorphism of Aragonite to Calcite. *Sedimentology* 56 (5), 1433–1463. doi:10.1111/j.1365-3091.2008.01041.x

Wright, D. T. (1999). The Role of Sulphate-Reducing Bacteria and Cyanobacteria in Dolomite Formation in Distal Ephemeral Lakes of the Coorong Region, South Australia. *Sediment. Geol.* 126 (1-4), 147–157. doi:10.1016/S0037-0738(99)00037-8

Wu, Y., Tahmasebi, P., Lin, C., and Dong, C. (2020a). A Comprehensive Investigation of the Effects of Organic-Matter Pores on Shale Properties: A Multicomponent and Multiscale Modeling. *J. Nat. Gas Sci. Eng.* 81, 103425. doi:10.1016/j.jngse.2020.103425

Wu, Y., Tahmasebi, P., Lin, C., and Dong, C. (2020b). Process-based and Dynamic 2D Modeling of Shale Samples: Considering the Geology and Pore-System Evolution. *Int. J. Coal Geol.* 218, 103368. doi:10.1016/J.COAL.2019.103368

Wu, Y., Tahmasebi, P., Lin, C., Zahid, M. A., Dong, C., Golab, A. N., et al. (2019). A Comprehensive Study on Geometric, Topological and Fractal Characterizations of Pore Systems in Low-Permeability Reservoirs Based on SEM, MICP, NMR, and X-Ray CT Experiments. *Mar. Petroleum Geol.* 103, 12–28. doi:10.1016/j.marpetgeo.2019.02.003

Yang, X., Li, Y., Zhan, Y., Huo, F., and Wang, X. (2021). Genesis of the Ordovician Ma55 Sub-member Dolomites in the Ordos Basin, China. *Carbonates Evaporites* 36 (2), 1–17. doi:10.1007/s13146-021-00699-5

Yuan, W., Chen, S., and Zeng, C. (2006). Study on Marine Transgression of Paleogene Shahejie Formation in Jiyang Depression. *Acta Pet. Sin.* 27 (4), 40. doi:10.14027/j.issn.1000-0550.2021.004

Zeng, F., Dong, C., Lin, C., Tian, S., Wu, Y., Lin, J., et al. (2021a). Pore Structure Characteristics of Reservoirs of Xihu Sag in East China Sea Shelf Basin Based on Dual Resolution X-Ray Computed Tomography and Their Influence on Permeability. *Energy* 239, 122386. doi:10.1016/j.energy.2021.122386

Zeng, F., Dong, C., Lin, C., Wu, Y., Tian, S., Zhang, X., et al. (2021b). Analyzing the Effects of Multi-Scale Pore Systems on Reservoir Properties-A Case Study on Xihu Depression, East China Sea Shelf Basin, China. *J. Petroleum Sci. Eng.* 203, 108609. doi:10.1016/j.petrol.2021.108609

Zhao, K., Du, X., Lu, Y., Xiong, S., and Wang, Y. (2019). Are Light-Dark Coupled Laminae in Lacustrine Shale Seasonally Controlled? A Case Study Using Astronomical Tuning from 42.2 to 45.4 Ma in the Dongying Depression, Bohai Bay Basin, Eastern China. *Palaeogeogr. Palaeoclimatol. Palaeoecol.* 528, 35–49. doi:10.1016/j.palaeo.2019.04.034

Zhu, G., Jin, Q., Dai, J., Guo, C., Zhang, L., and Li, J. (2004). A Study on Periods of Hydrocarbon Accumulation and Distribution Pattern of Oil and Gas Pools in Dongying Depression. *Oil Gas Geol.* 25 (2), 209–215.

Conflict of Interest: YH was employed by the company CNOOC Tianjin Company. WL was employed by the company Oil and Gas Survey.

The remaining authors declare that the research was conducted in the absence of any commercial or financial relationships that could be construed as a potential conflict of interest.